MFiX Application to Circulating Fluid Bed Boiler

Subhodeep Banerjee[1,2], Mehrdad Shahnam[1], William A. Rogers[1]

[1] National Energy Technology Laboratory, 3610 Collins Ferry Road, Morgantown, WV 26505
[2] Leidos Research Support Team, 3610 Collins Ferry Road, Morgantown, WV 26505

November 6, 2020

Solutions for Today | Options for Tomorrow

Motivation

- Circulating fluidized bed (CFB) boilers as a power generation technology offers several advantages
  - Increased gas-solid mixing resulting in higher efficiency
  - Increased fuel flexibility
  - Reduced NO_x emissions due to lower temperature operation

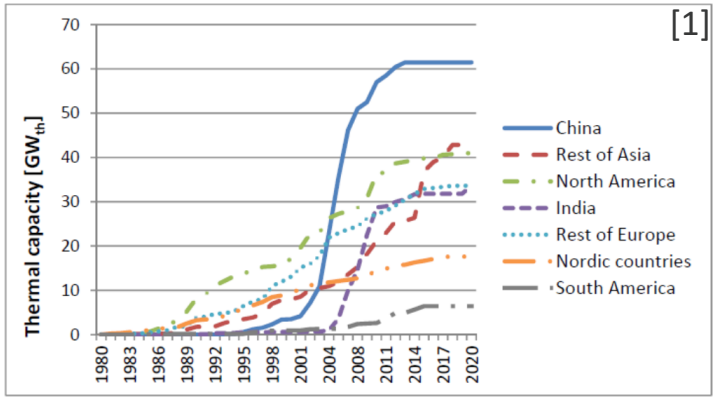

- Over the last decade, bioenergy increased from 8% of the world's total primary energy supply to 10%, and it has been projected to rise further to 25–33% by 2050[2]
- Comprehensive CFD model of a CFB boiler must include hydrodynamics, wall heat transfer model, and combustion models
- Bulk of numerical models in literature has been limited to hydrodynamics only or focused on oxy-fuel combustion

[1] Leckner, B. et al., 2016. Utilization of fluidized bed boilers—a worldwide overview. In 73rd IEA-FBC Technical Meeting. Tokyo, Japan, 2016.
[2] Energy Information Administration, 2013. *International Energy Outlook 2013*. Washington, DC: U.S. Department of Energy.

50kW$_{th}$ CFB Combustor Experiment

- Bench-scale experimental facility designed, built, and operated at CanmetENERGY, Natural Resources Canada[1] (NRCan)

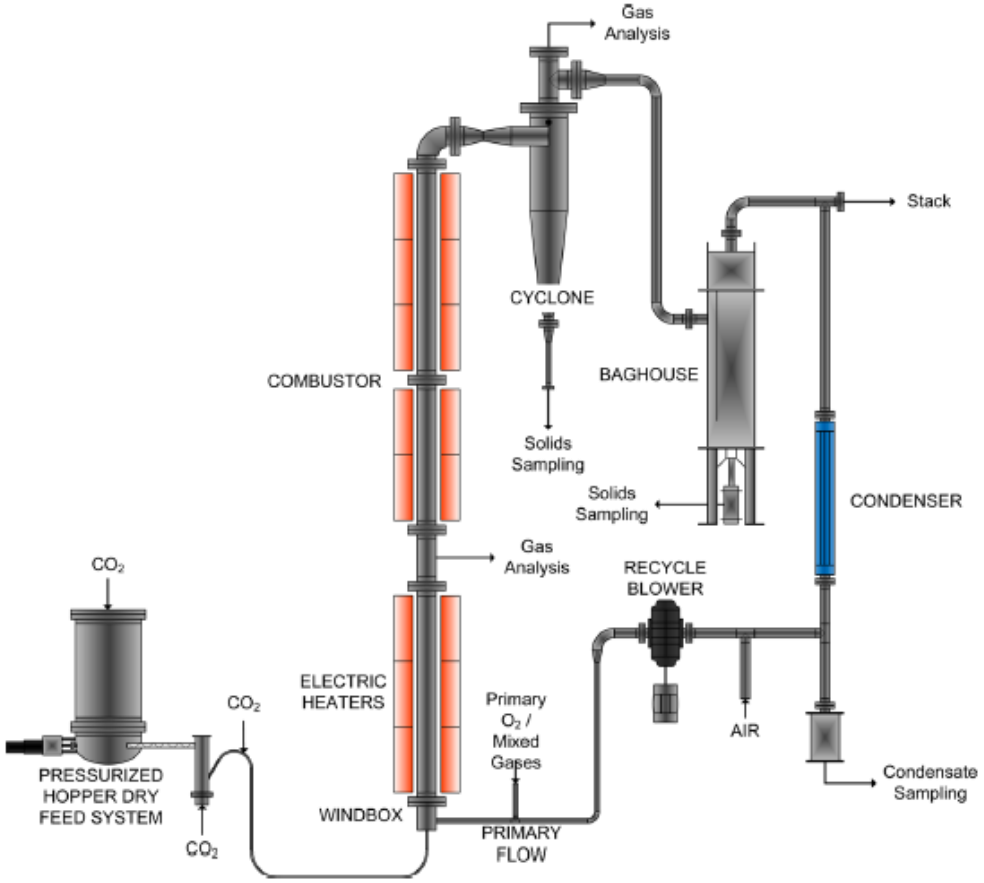

Operating Conditions	
Inert material	Olivine sand, 273 µm, 3063 kg/m³
Biomass	Torrefied hardwood, 375 µm, 520 kg/m³
Initial mass of inert	9.0 kg
$\dot{m}$ of fluidizing gas (air)	15.6 kg/h
$\dot{m}$ of fuel feed gas (air)	3.06 kg/h
$\dot{m}$ of biomass	2.65 kg/h
Sidewall temperature	850°C
Fluidizing gas inlet temperature	120°C
Fuel feed gas inlet temperature	20°C

[1] Hughes, R.W. et al., 2015. Oxy-fluidized bed combustion using under bed fines fuel injection. In 22nd International Conference on Fluidized Bed Conversion. Turku, Finland, 2015.

Experimental Conditions and Results

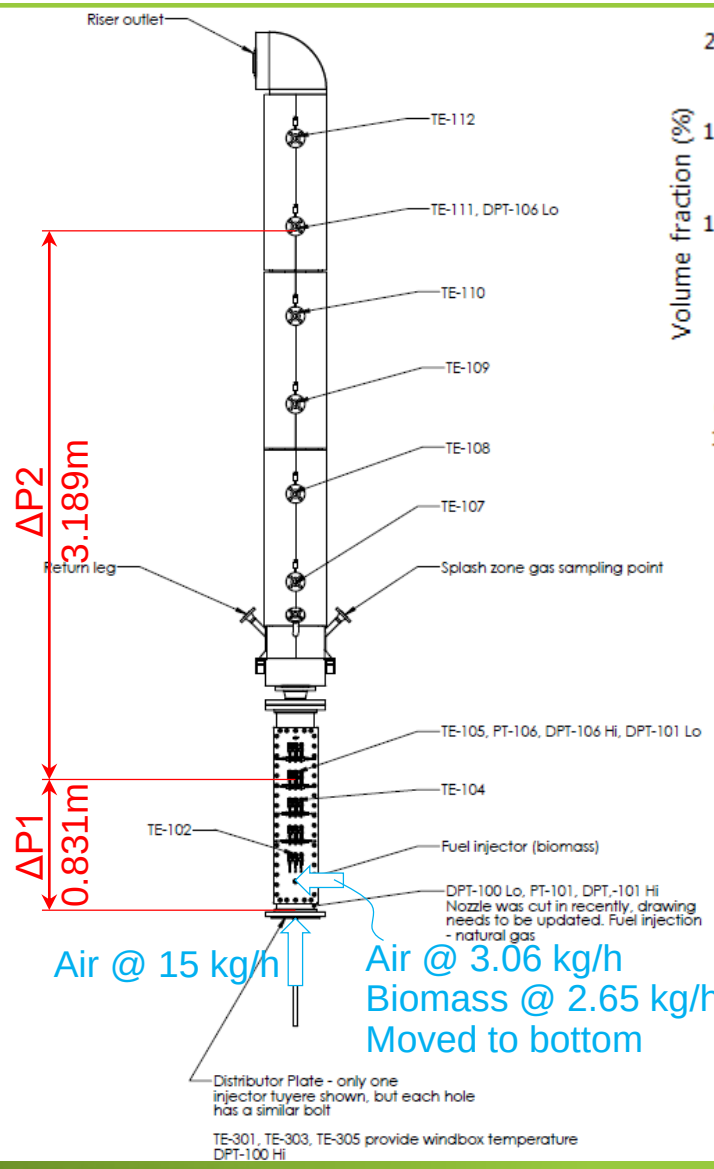

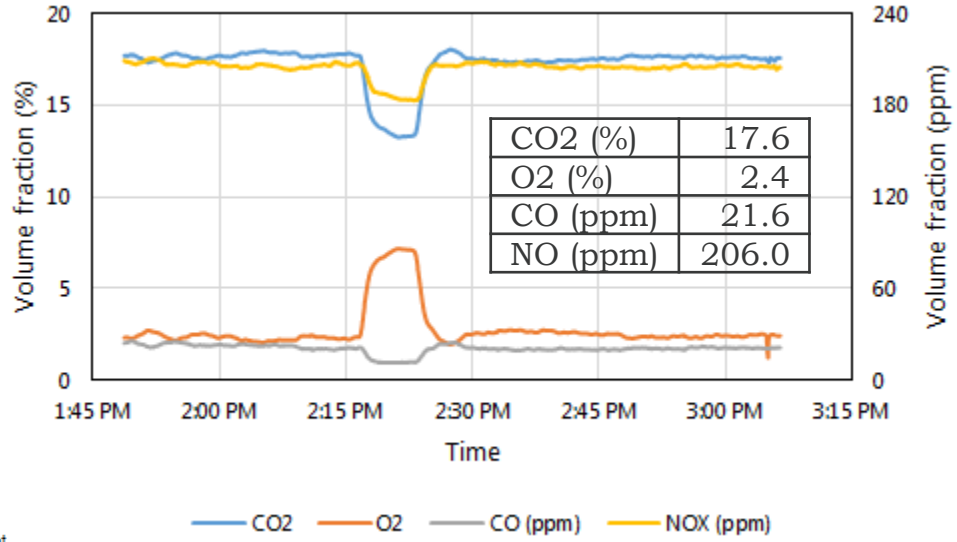

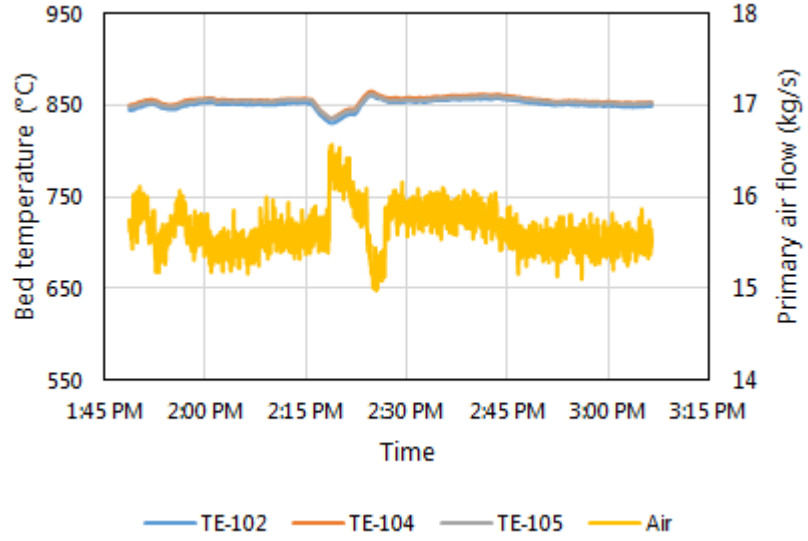

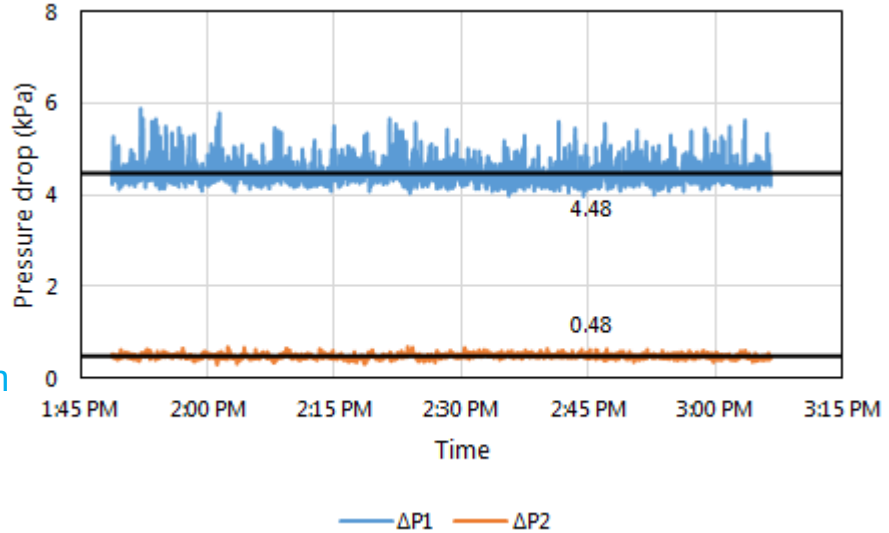

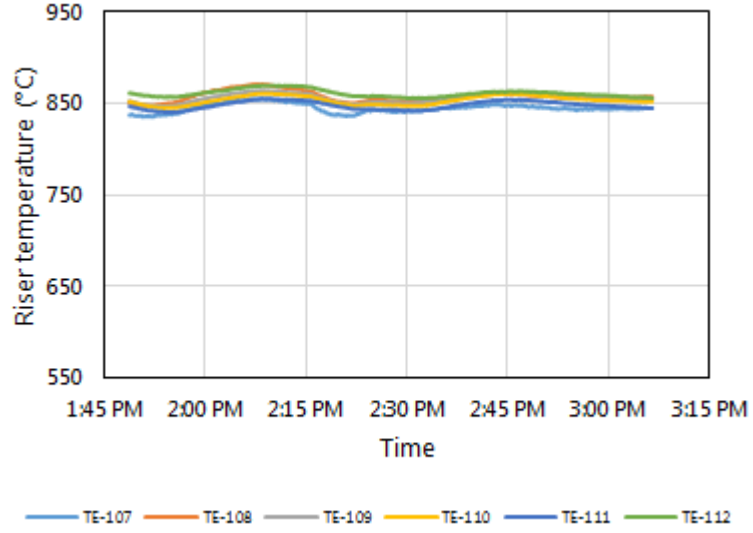

Numerical Solution Approach

- The NRCan experiment is modeled using the multi-phase particle-in-cell (PIC) approach in the open-source MFiX Software Suite v20.2[1]
- A Cartesian grid is used to discretize the computational domain of the riser into 0.005m × 0.008m × 0.005m cells with boundary cells truncated to conform to the domain surface (cut-cell approach)
- The individual sand and biomass particles are grouped into parcels with a statistical weight of 500 ($d_{parcel} = 7.937 \cdot d_{particle}$)
- Simulations are run on the NETL supercomputer Joule 2.0 using distributed memory parallel through message passing interface

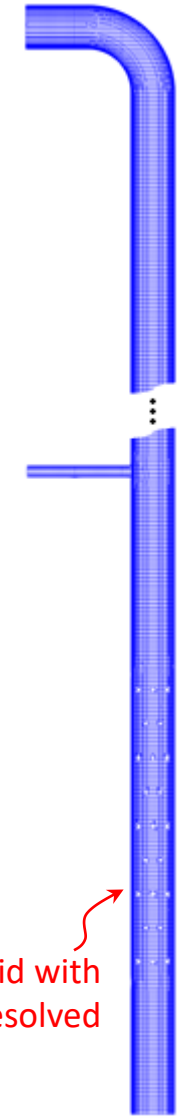

Computational grid with tube bank resolved

[1] MFS Development Group, 2020. *The MFiX 20.2 User Guide, Release 20.2.0*. Morgantown, WV: Department of Energy. (https://mfix.netl.doe.gov/)

Governing Equations

- Fluid phase
  - $\frac{\partial}{\partial t}\left(\varepsilon_f \rho_f\right) + \nabla \cdot \left(\varepsilon_f \rho_f \boldsymbol{u}_f\right) = \dot{m}_{sg}$
  - $\frac{\partial}{\partial t}\left(\varepsilon_f \rho_f \boldsymbol{u}_f\right) + \nabla \cdot \left(\varepsilon_f \rho_f \boldsymbol{u}_f \boldsymbol{u}_f\right) = -\varepsilon_f \nabla p_f - \nabla \cdot \bar{\bar{\tau}}_f + \varepsilon_f \rho_f \mathbf{g} - \boldsymbol{K}_{sg}$
  - $\frac{\partial}{\partial t}\left(\varepsilon_f \rho_f E\right) + \nabla \cdot \left(\varepsilon_f \boldsymbol{u}_f \left(\rho_f E + p_f\right)\right) = \nabla \cdot \left(k \nabla T - \sum h_j \boldsymbol{J}_j + \left(\bar{\bar{\tau}}_f \cdot \boldsymbol{u}_f\right)\right) + S_h$
- Fluid phase stress tensor
  - $\bar{\bar{\tau}}_f = \mu_f \left(\nabla \boldsymbol{u}_f + \nabla \boldsymbol{u}_f^T\right) - \frac{2}{3} \mu_f \nabla \boldsymbol{u}_f \bar{\bar{I}}$
- Solid phase
  - $\frac{d\boldsymbol{x}_p}{dt} = \boldsymbol{u}_p$
  - $\frac{d\boldsymbol{u}_p}{dt} = -\frac{\nabla p}{\rho_p} + \mathbf{F}_{drag} + \mathbf{F}_{contact} + \mathbf{g}$

Governing Equations

- Drag force accounts for solid-gas momentum exchange
  - $\boldsymbol{F}_{drag} = F_D(\boldsymbol{u}_f - \boldsymbol{u}_p)$
  - $F_D = \frac{18\mu_f}{\rho_p d_p^2}\frac{C_D Re_p}{24}$
  - $Re_p = \frac{\rho_f d_p |\boldsymbol{u}_f - \boldsymbol{u}_p|}{\mu_f}$
- Source term in fluid momentum equation $\boldsymbol{K}_{sg} = \beta_{sg}(\boldsymbol{u}_f - \boldsymbol{u}_p)$
  - For $\varepsilon_s > 0.8$, $\beta_{sg} = \frac{3}{4} C_D \frac{\varepsilon_s \varepsilon_g \rho_g |\boldsymbol{u}_f - \boldsymbol{u}_p|}{d_p} \varepsilon_g^{-2.65}$; $C_D = \frac{24}{\varepsilon_g \mathrm{Re}_p}\left[1 + 0.15(\varepsilon_g \mathrm{Re}_p)^{0.687}\right]$
  - For $\varepsilon_s \leq 0.8$, $\beta_{sg} = 150\frac{\varepsilon_s(1-\varepsilon_g)\mu_g}{\varepsilon_g d_p^2} + 1.75\frac{\rho_g \varepsilon_s |\boldsymbol{u}_f - \boldsymbol{u}_p|}{d_p}$

  Gidaspow[1]
- Contact force accounts for interparticle interactions
  - $\mathbf{F}_{contact} = \frac{\nabla \bar{\bar{\tau}}_s}{\varepsilon_s \rho_p}$
  - $\bar{\bar{\tau}}_s = \frac{P_p \varepsilon_s^{\gamma}}{\max[(\varepsilon_{cp} - \varepsilon_s), \delta(1-\varepsilon_s)]}$

[1] Gidaspow, D., 1992. *Multiphase Flow and Fluidization*. San Diego, CA: Academic Press.

Hydrodynamics Benchmarking

- Cold flow experiments are conducted with 9.0 kg of olivine sand fluidized by air with no biomass feed
- Temperature of fluidizing air is set at 120°C to match reacting flow experiments

	Non-circulating			Circulating		w/RXNs
U (m/s)	0.40	0.70	1.56	3.09	5.94	15.65
U/U_{mf}	5.28	9.30	20.82	41.09	77.98	-
T_{avg} (°C)	120.8	120.0	124.0	122.7	115.2	850
ΔP1 (kPa)	7.8	7.8	6.8	3.9	0.1	4.3
ΔP2 (kPa)	0.0	0.0	0.0	0.8	1.2	0.5

- At low fluidization velocities, the bed is in the bubbling fluidization regime with no circulation
- U = 3.09 m/s has the closest pressure drop to the biomass combustion experiments so this case is used to determine the optimum PIC parameters P_p and γ

Particle Recirculation Algorithm

- For U = 3.09 m/s, olivine particles are elutriated out of the riser and recirculation of sand must be considered to maintain accurate inventory for comparison with experiment
- The non-reacting simulation is initialized with 9.0 kg of olivine and allowed to evolve until a prescribed recirculating inventory of 4.5 kg is reached
- Once recirculating inventory is achieved, any additional particles leaving the riser are looped back in at the side inlet with a constant axial velocity to maintain the prescribed inventory
- The recirculating inventory has a different size distribution compared to the original sample

Hydrodynamics Benchmarking

U = 3.09 m/s

- Pressure fluctuations achieve pseudo-steady-state quickly after recirculating inventory is achieved
- P_p and γ has strong effect on PSD of recirculating inventory, which cancels out the effect on the overall pressure drop in the riser

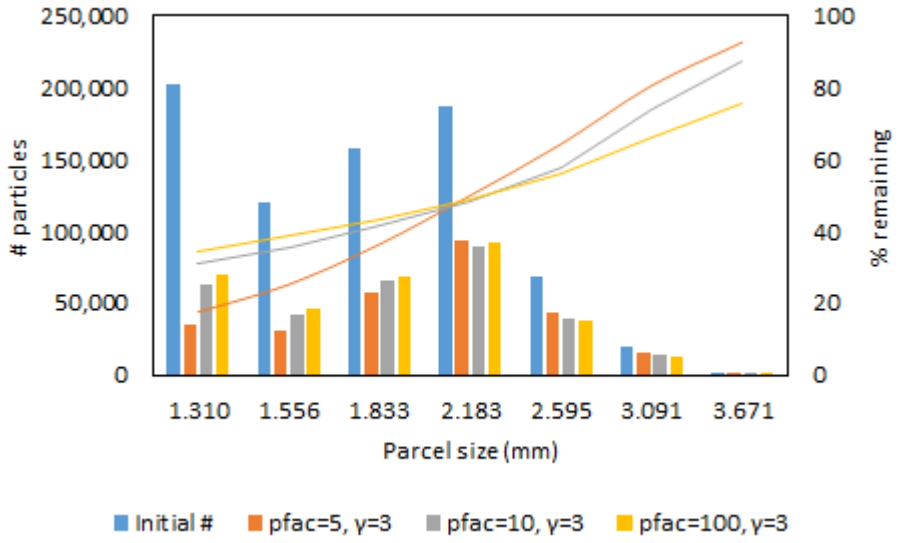

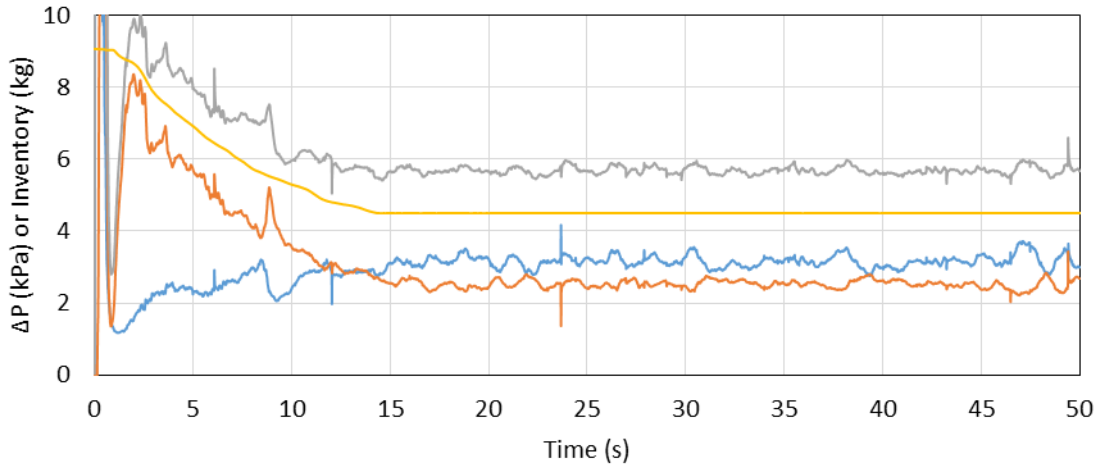

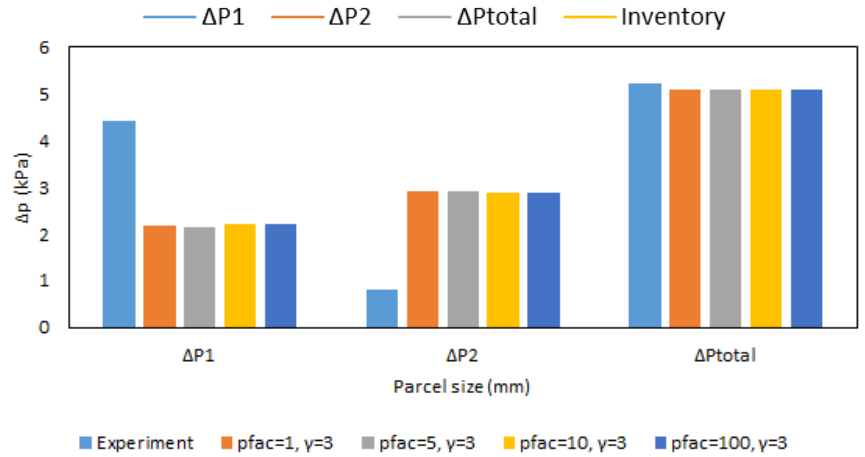

- P_p = 10, γ = 3 provides a balance between elutriation of small and large particles

Hydrodynamics Benchmarking – Effect of Drag Model

- Several sub-grid (filtered) drag models have been proposed in the literature to overcome the limitations of homogeneous drag models to capture mesoscale effects when the grid size is coarse
- Homogeneous drag models such as Gidaspow can correctly predict the fluidization behavior when the grid size is 2-4 times the particle diameter for bubbling fluidized beds or up to 10 times for circulating fluidized beds, but their performance start to degrade when coarse-graining the model by combining individual particles into parcels
- A comparative study[1] of eight drag models, three homogeneous and five heterogeneous, demonstrated the need to modify the homogeneous models to account for the mesoscale structures to achieve accurate drag prediction in coarse grid simulations
- The enhanced Sarkar drag model[1] was previously shown to achieve superior prediction across all fluidization regimes compared to homogeneous drag models and other heterogeneous drag models

[1] Gao, X., Li, T., Sarkar, A., Lu, L. and Rogers, W.A. (2018) Development and validation of an enhanced filtered drag model for simulating gas-solid fluidization of Geldart A particles in all flow regimes, *Chemical Engineering Science*, 184, pp. 33–51.

Hydrodynamics Benchmarking – Effect of Drag Model

- Fluidization is impeded by applying the filtered drag model, so more particles are retained in the lower riser
- Circulation rate is reduced, reflected in the average mass of recirculated particles in the side inlet
- Pressure drop distribution and overall pressure drop using the filtered drag model show better agreement with the experimental results (P_p = 10, γ = 3)

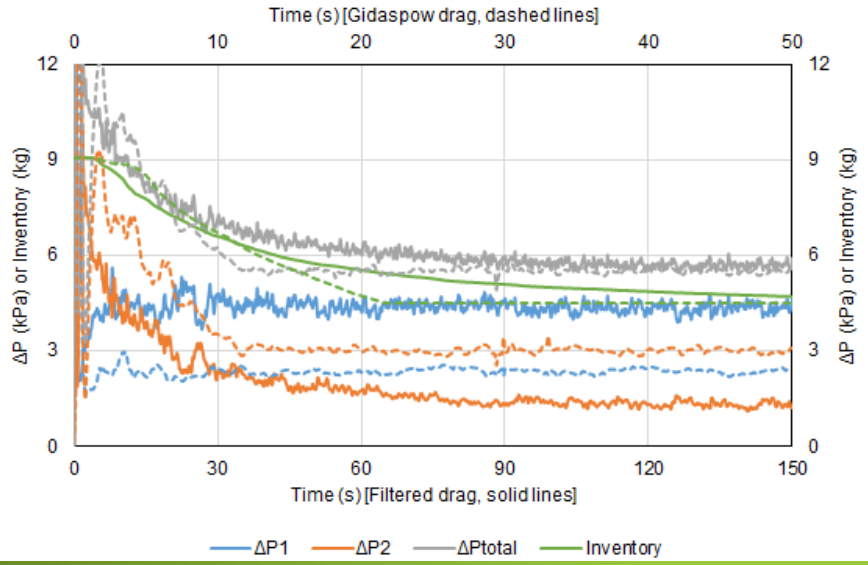

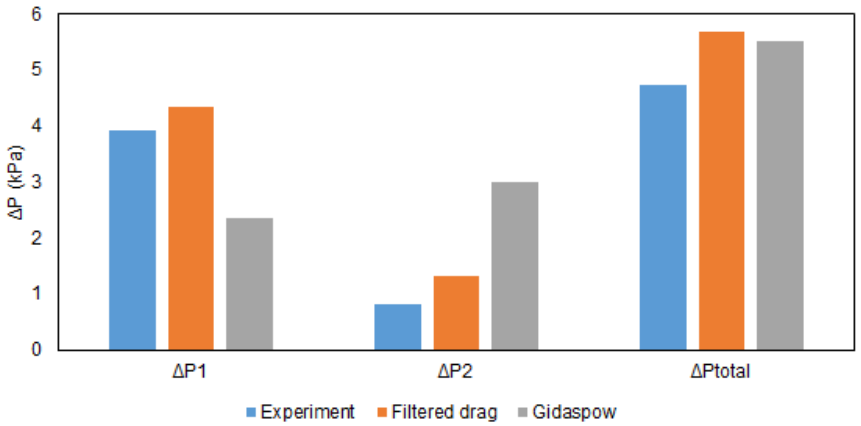

First 5s shown

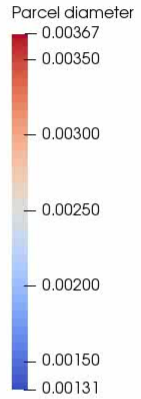

Full Loop Simulation

- From the riser-only simulations, the experimental pressure drop distribution in the riser can be matched *as long as* the riser holdup matches the experiment
- It is desirable to model the full loop so that the riser holdup can be allowed to evolve as a function of the operating parameters instead of being fixed at a prescribed value

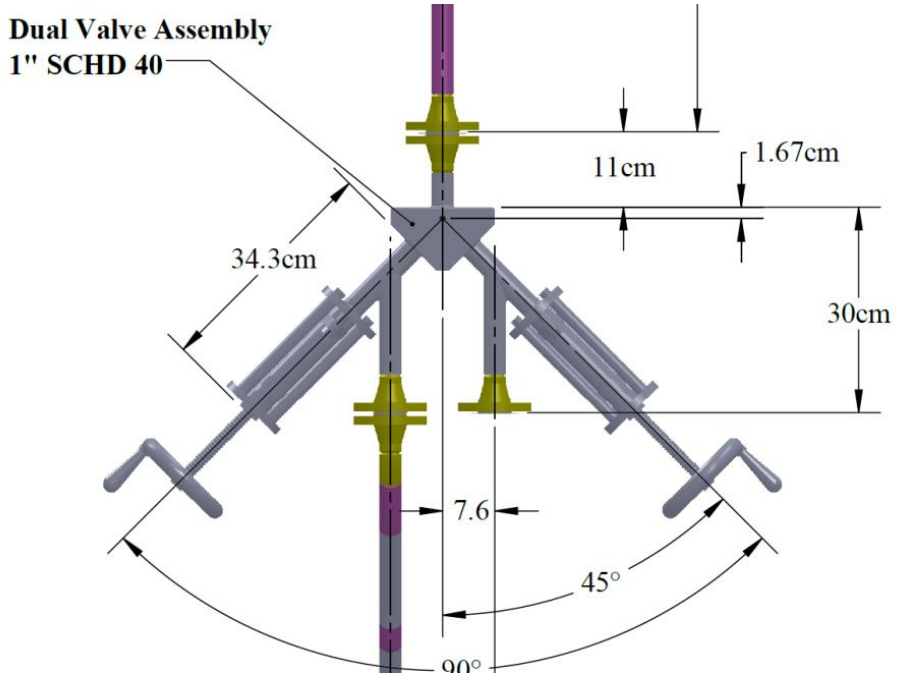

Particle recirculation mechanism is via a ram valve

Full Loop Simulation

U = 3.09 m/s, filtered drag model

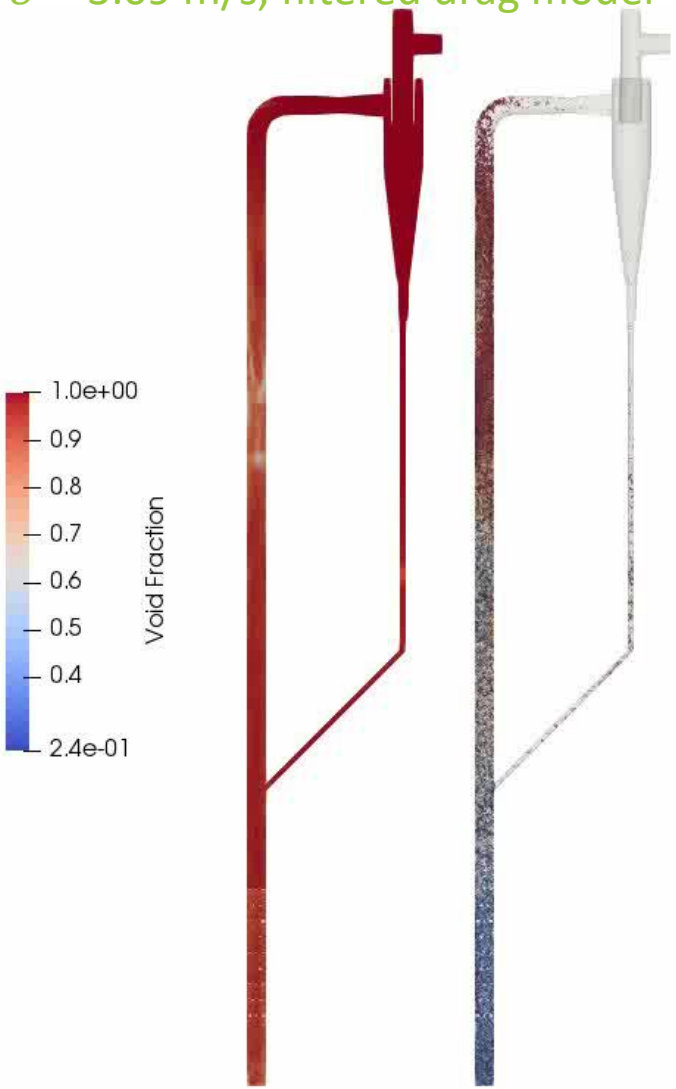

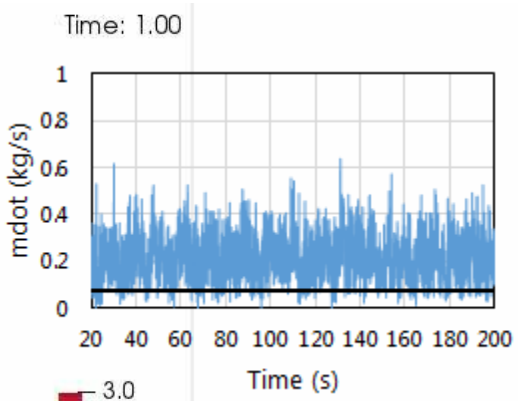

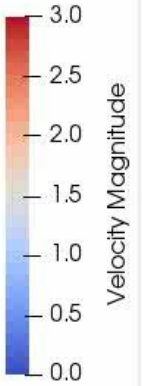

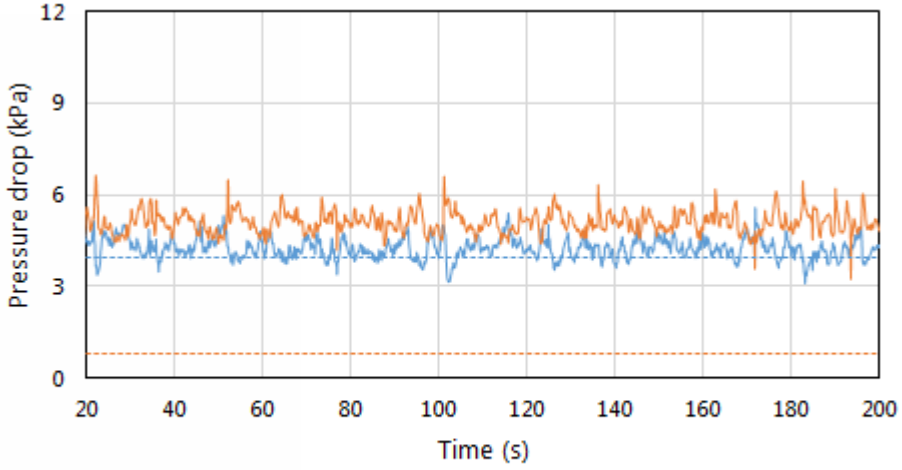

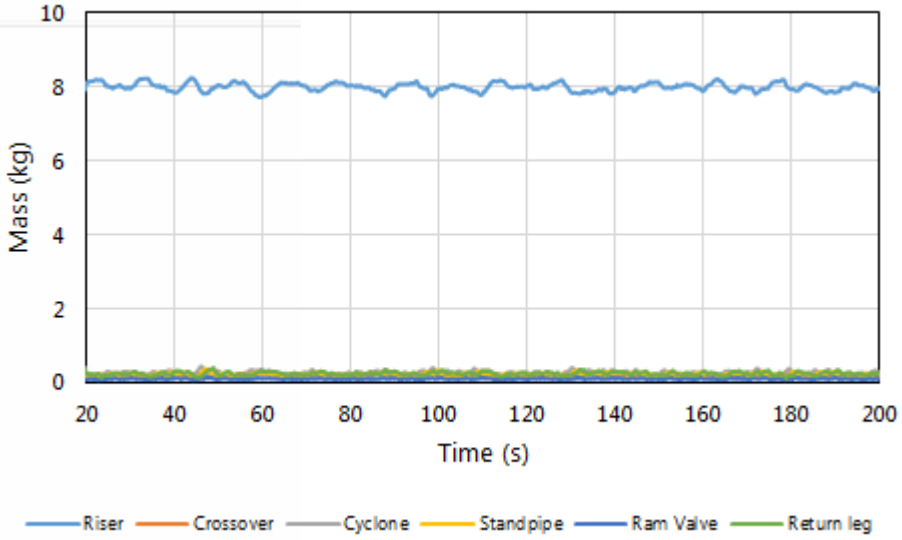

Full Loop Simulation – Effect of Drag Model

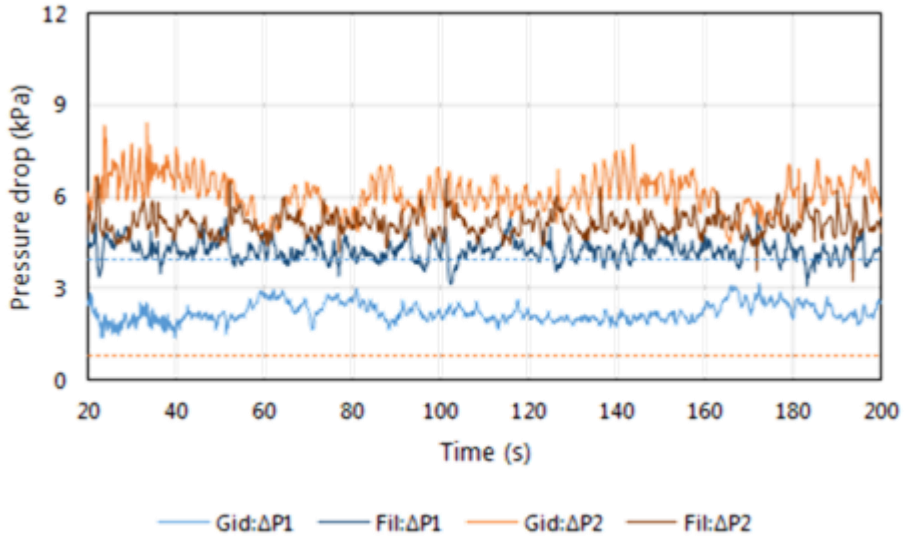

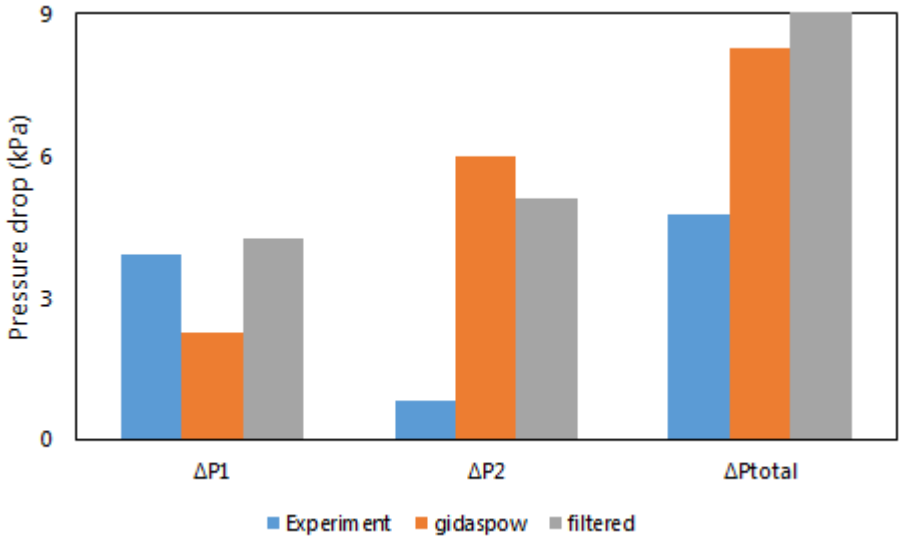

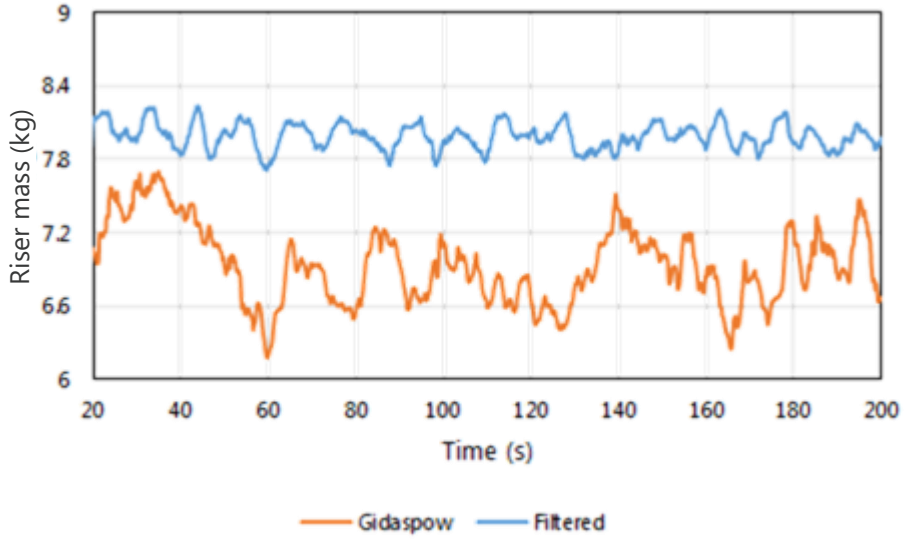

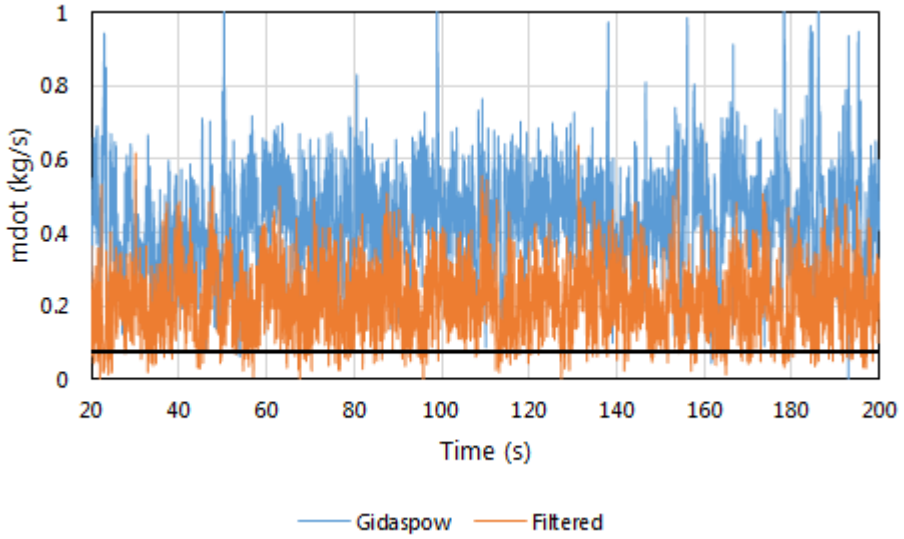

	Exp.	Gid.	Fil.
ΔP_1 (kPa)	3.92	2.27	4.23
ΔP_2 (kPa)	0.82	5.99	5.11
ΔP_T (kPa)	4.74	8.26	9.35
m_{riser} (kg)	–	6.87	7.98
$\dot{m}$ (kg/s)	–	0.45	0.22

- The PIC model is unable to replicate the close packing in the standpipe, so residence time in the standpipe is minimal
- The residence time can be increased by partially closing the ram valve, thereby approximating the dense packing in the standpipe

Full Loop Simulation with Valve Partially Closed

Full Loop Simulation with Valve Partially Closed

Valve stroke = 34 mm

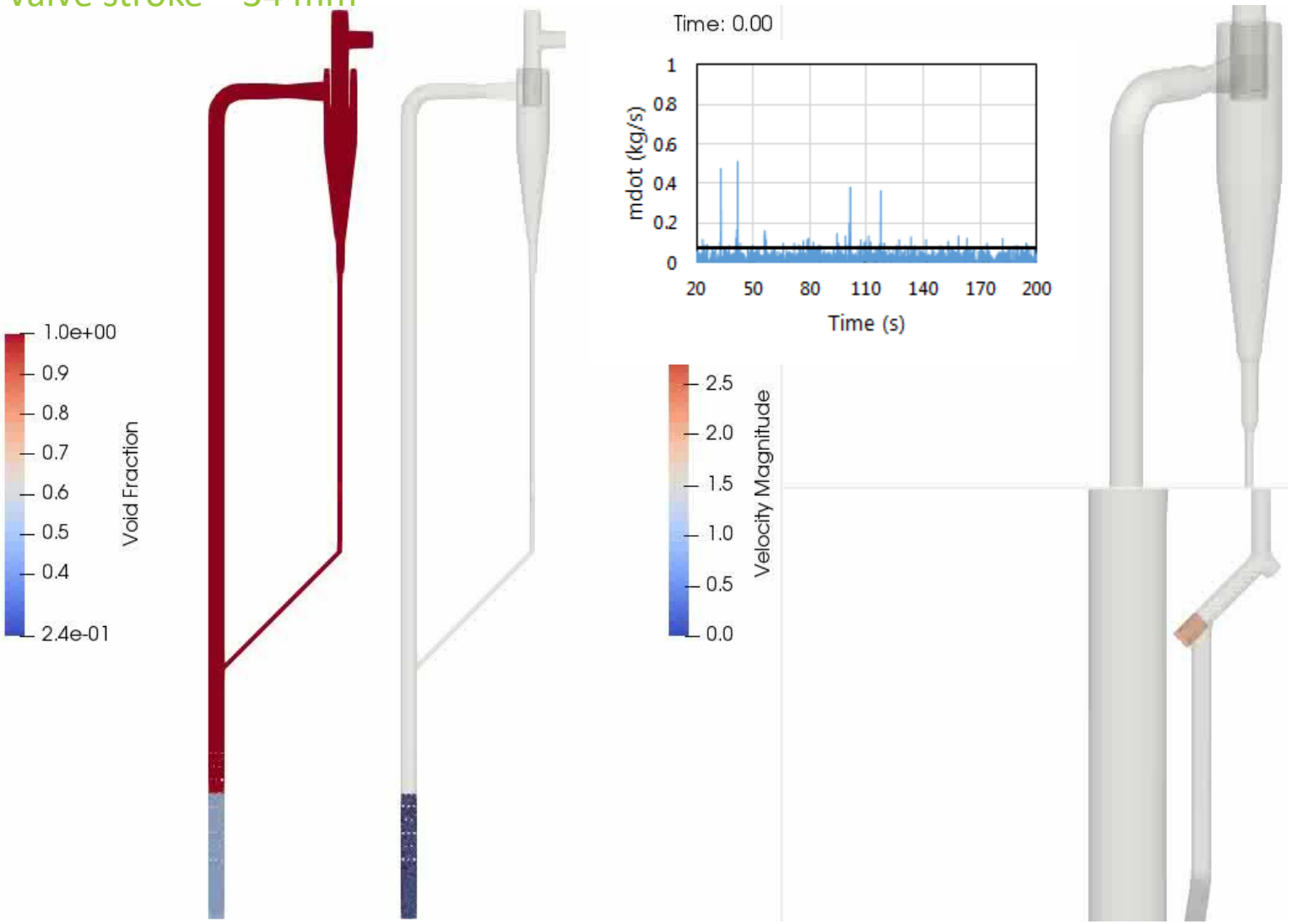

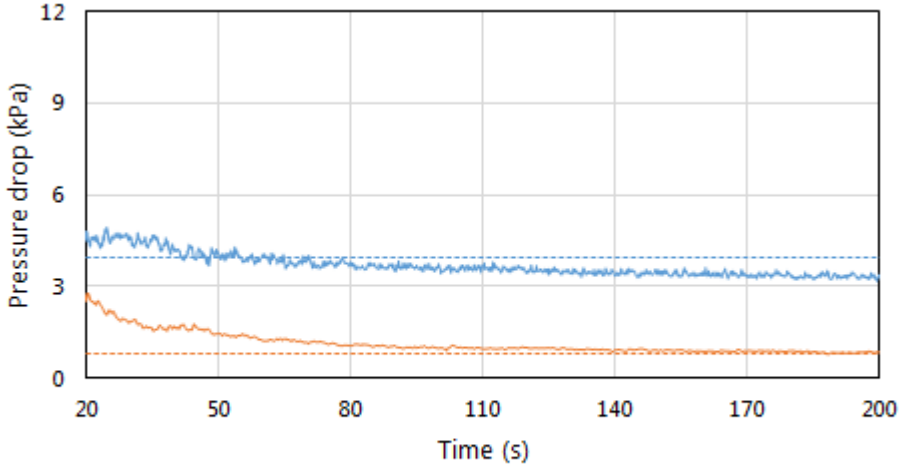

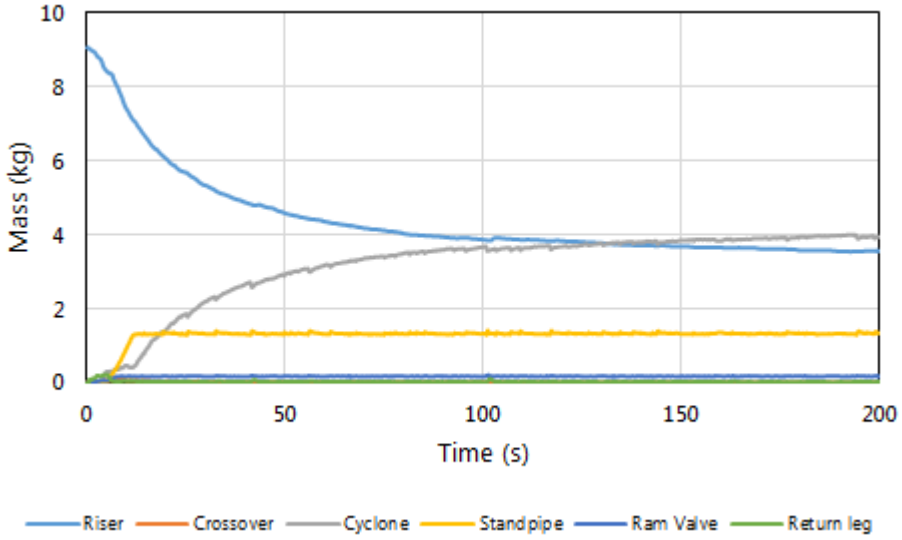

Biomass Composition

Moisture	3.68
Ash	1.12
Volatile matter	74.03
Fixed carbon	21.17

Carbon	51.40
Hydrogen	5.77
Nitrogen	0.16
Sulfur	0.05
Oxygen	37.82

- Assuming the fixed carbon comprises pure C, and ignoring trace amounts of N and S, the elemental ratios of C, H, and O can be used to determine the composition of the pseudo-species

Volatile matter	74.03

Carbon	30.23
Hydrogen	5.77
Oxygen	37.82

- Empirical formula: $CH_{2.274}O_{0.9392}$

Volatiles as a Lumped Species

- For combustion simulations, the volatile gases can be lumped into a single "artificial" species, CH_xO_y[1]
- The simplest reaction mechanism to model the volatile matter combustion is the global one-step reaction[2,3]

$$CH_xO_y + \left(1 + \frac{x}{4} - \frac{y}{2}\right) O_2 \rightarrow CO_2 + \frac{x}{2} H_2O$$

- A more accurate approach is provided by the global two-step reaction mechanism which treats CO as an intermediate species[3]

$$CH_xO_y + \left(\frac{1}{2} + \frac{x}{4} - \frac{y}{2}\right) O_2 \rightarrow CO + \frac{x}{2} H_2O;\ CO + \frac{1}{2} O_2 \rightarrow CO_2$$

- ΔH_r obtained from heating value of fuel *less* contributions from other reactions

[1] Marangwanda, G.T., Madyira, D.M. & Babarinde, T.O. (2020) Combustion models for biomass: A review. *Energy Reports*, 6, pp. 664–672.
[2] Ma, L., Jones, J.M., Pourkashanian, M. & Williams, A. (2007) Modelling the combustion of pulverized biomass in an industrial combustion test furnace. *Fuel*, 86, 1959–1965.
[3] Álvarez, L., Yin, C., Riaza, J., Pevida, C., Pis, J.J. & Rubiera, F. (2014) Biomass co-firing under oxy-fuel conditions: A computational fluid dynamics modelling study and experimental validation. *Fuel Process. Technol.*, 120, pp. 22–33.
[4] Tabet, F. & Gökalp, I. (2015) Review on CFD based models for co-firing coal and biomass. *Renew. Sust. Energ. Rev.*, 51, 1101–1114.

Volatiles as a Lumped Species

- Reaction rate kinetics for the global one-step and two-step mechanisms can be roughly approximated from Westbrook & Dryer[1]

$$k = A \cdot T^n \cdot \exp\left(-\frac{E_a}{R \cdot T}\right) \cdot [\text{Fuel}]^a \cdot [\text{Oxidizer}]^b$$

(units are cm-sec-mole-kcal-Kelvins)

Fuel	A	Ea	a	b
CH_4	1.3×10^8	48.4	−0.3	1.3
CH_4	8.3×10^5	30.0	−0.3	1.3
C_2H_6	1.1×10^{12}	30.0	0.1	1.65
C_3H_8	8.6×10^{11}	30.0	0.1	1.65
C_4H_{10}	7.4×10^{11}	30.0	0.15	1.6
C_5H_{12}	6.4×10^{11}	30.0	0.25	1.5
C_6H_{14}	5.7×10^{11}	30.0	0.25	1.5
C_7H_{16}	5.1×10^{11}	30.0	0.25	1.5
C_8H_{18}	4.6×10^{11}	30.0	0.25	1.5
C_8H_{16}	7.2×10^{12}	40.0	0.25	1.5
C_9H_{20}	4.2×10^{11}	30.0	0.25	1.5
$C_{10}H_{22}$	3.8×10^{11}	30.0	0.25	1.5
CH_3OH	3.2×10^{12}	30.0	0.25	1.5
C_2H_5OH	1.5×10^{12}	30.0	0.15	1.6
C_6H_6	2.0×10^{11}	30.0	−0.1	1.85
C_7H_8	1.6×10^{11}	30.0	−0.1	1.85
C_2H_4	2.0×10^{12}	30.0	0.1	1.65
C_3H_6	4.2×10^{11}	30.0	−0.1	1.85
C_2H_2	6.5×10^{12}	30.0	−0.2	1.25

Volatiles species slots in here by C/H ratio

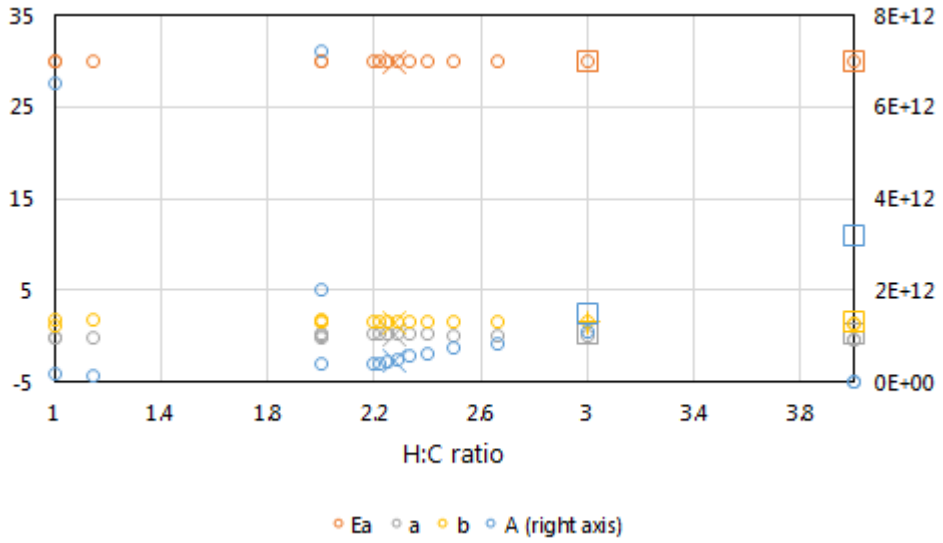

- Hence, $k = 4.94 \cdot 10^{11} \cdot \exp(-1.510 \cdot 10^4/T) \cdot [\text{Volatiles}]^{0.25} \cdot [O_2]^{1.5}$

[1] Westbrook, C.K. & Dryer, F.L. (1981) Simplified reaction mechanisms for the oxidation of hydrocarbon fuels in flames. *Combust. Sci. Technol.*, 27, pp. 31–43.

Simplified Chemical Reaction Scheme

Pyrolysis	$\text{Biomass}_{(s)} \rightarrow \text{Volatiles}_{(g)}$ [where volatiles = $CH_{2.274}O_{0.9392}$]	
Char combustion	$\text{Char}_{(s)} + O_2 \rightarrow CO_2$	
Volatile combustion	$CH_{2.274}O_{0.9392} + 1.099017 \cdot O_2 \rightarrow CO_2 + 1.137212 \cdot H_2O$	
Pyrolysis	$r_{pyrolysis} = 2 \times 10^{19}\, e^{\frac{-212180}{8.314 T_b}} \frac{m_b}{MW_b}$	Developed at NETL for Cypress hardwood
Char combustion	$r_{char} = \frac{p_{O_2} S_{char}}{MW_{O_2}[1/k_{film} + 1/k_{reaction} + 1/k_{ash}]}$	Wen et al. (1982)
Volatile combustion	$r_{H_2} = 4.94 \cdot 10^{11} e^{\frac{-15100}{T_g}} c_{O_2}^{1.5} c_{\text{Volatiles}}^{0.25}$	Derived from Westbrook and Dryer (1981)

Simplified Chemical Reaction Scheme Results

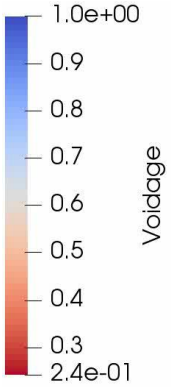

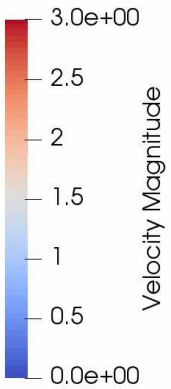

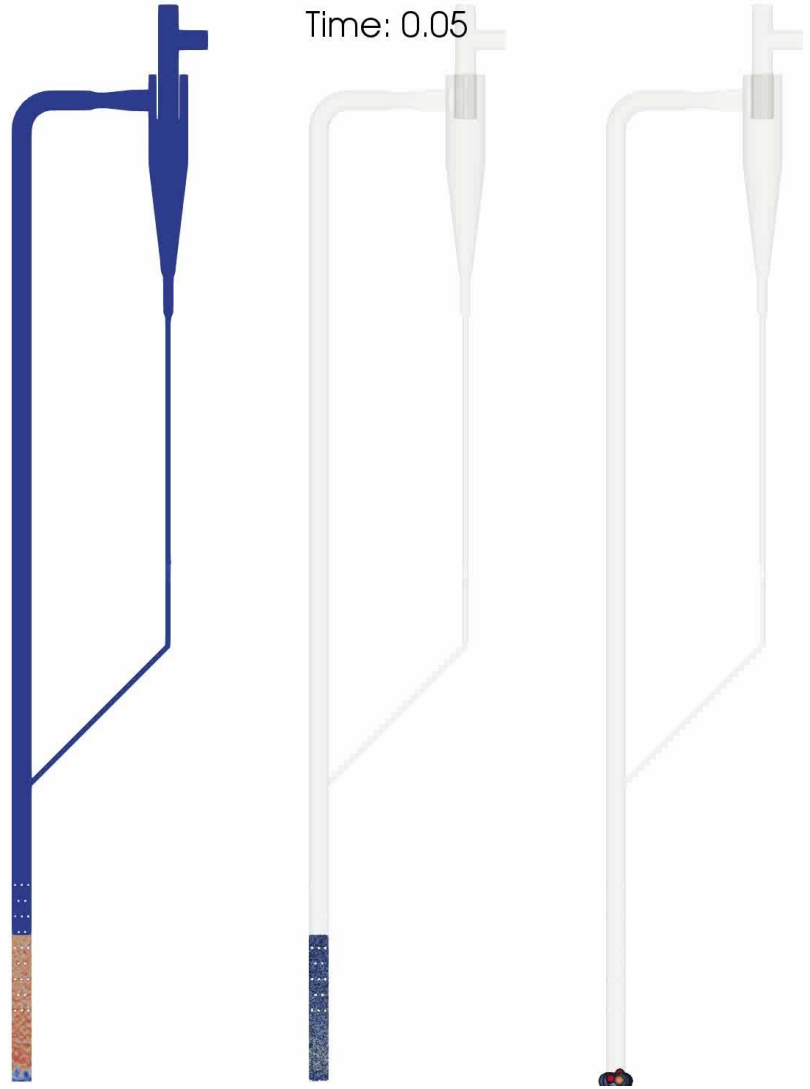

Total biomass inventory in the riser is negligible compared to sand inventory

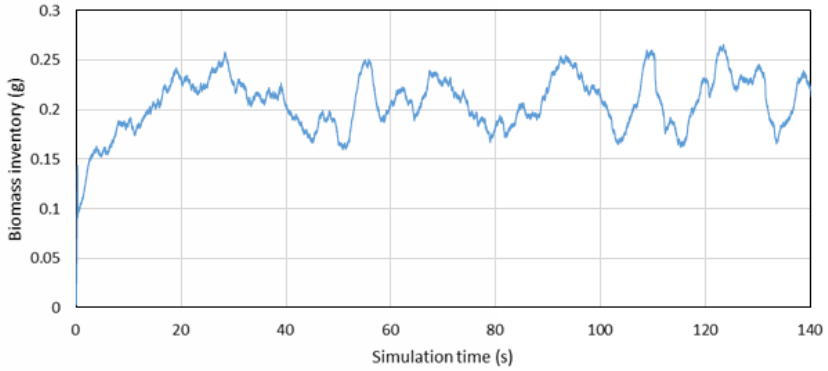

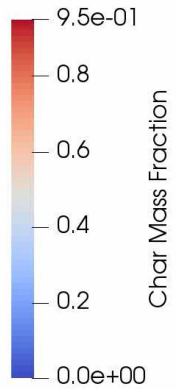

Simplified Chemical Reaction Scheme Results

- Bottom 1 m of riser magnified to highlight combustion zone
- Pyrolysis is near instantaneous at 850°C and occurs to completion near the inlet
- Next, pyrolysis vapors are combusted in the bottom bed region near the inlet
- Char combustion rates are highest in the stagnation zones around the heat exchanger tubes

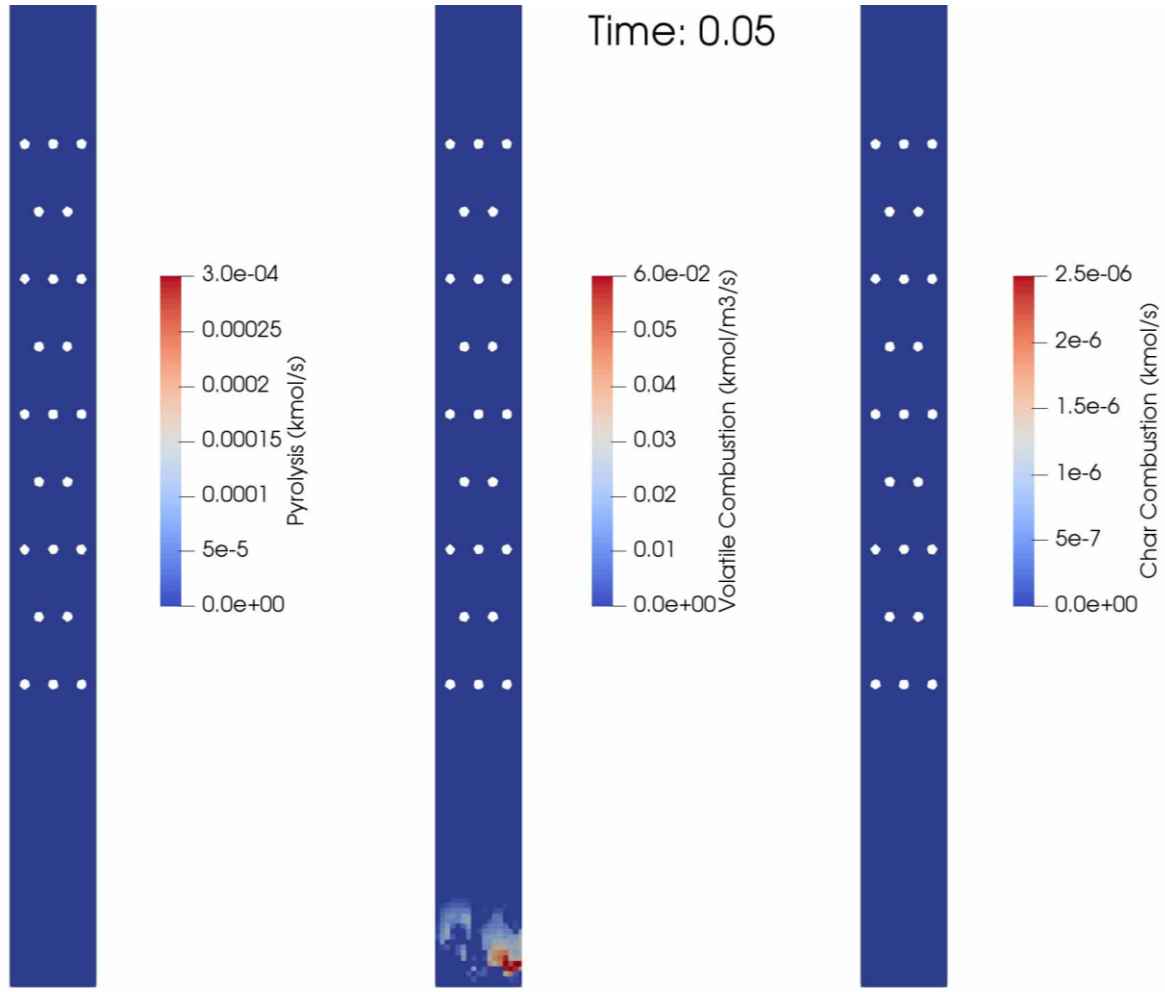

Simplified Chemical Reaction Scheme Results

- The outlet compositions of CO_2 and O_2 show excellent match with experimental results (dashed lines)

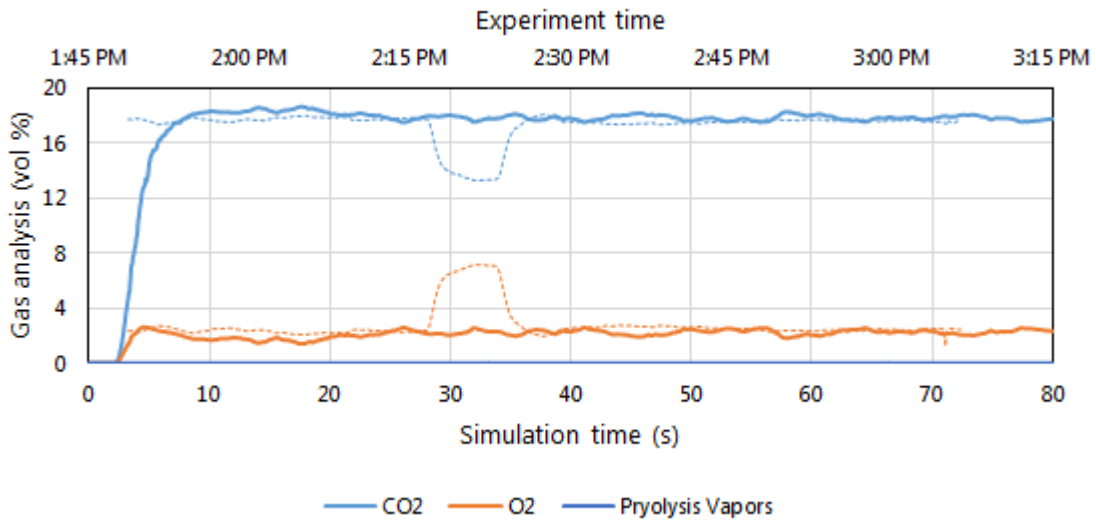

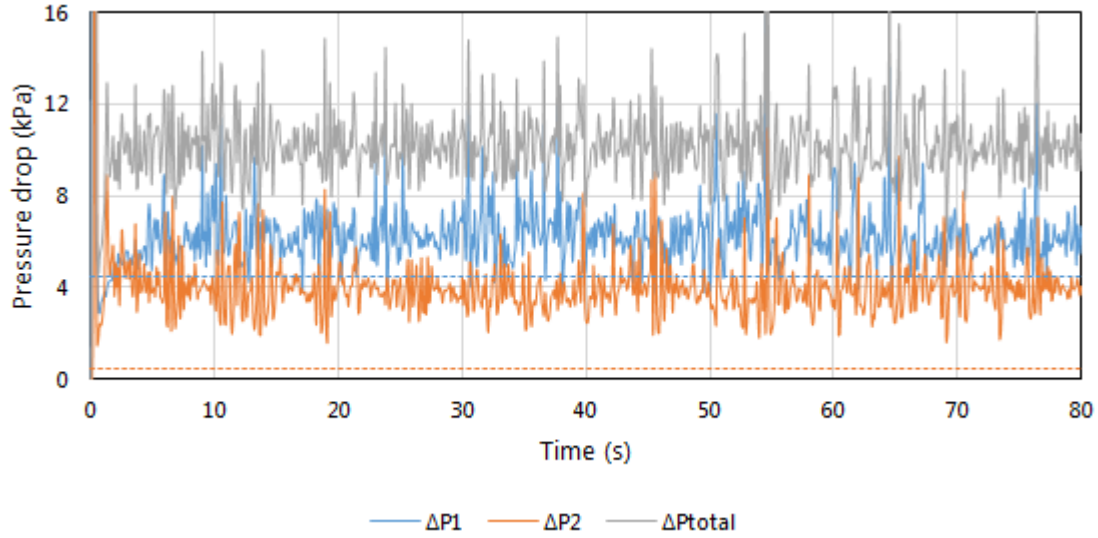

- Particle fluidization is reduced compared to cold flow simulations, leading to reduced circulation and higher particle holdup in riser, and hence higher pressure drops
  - Air flow of 15.6 kg/h corresponds to an inlet air velocity of 0.67 m/s, lower than the 3.09 m/s used in the cold flow simulations
  - Further investigation of hot flow hydrodynamics is required

Conclusions

- Hydrodynamics of the 50kW$_{th}$ riser at CanmetENERGY, Natural Resources Canada are validated against experiment via inert simulations using olivine sand
- Filter size dependent corrections to the homogeneous drag laws are incorporated to take into account the mesoscale effects such as bubbles and clusters to ensure accuracy
- In the full loop simulation, once the lower bed pressure drop matches the experiment, the upper riser pressure drop can be tuned independently of the lower bed by modeling pseudo-packing in the return leg by adjusting the ram valve stroke
- The validated cold flow model is extended to model reacting flow with torrefied hardwood as the feedstock and validate a simplified global one-step mechanism for combustion
- Species concentrations at the riser outlet are compared against the experiment and show excellent agreement
- The simulations demonstrate the ability of MFiX-PIC to accurately capture the physics and chemistry of a circulating fluidized bed combustor at bench scales, which can be further extended to pilot- and industrial-scale systems

Acknowledgments

- The presenter and NETL acknowledge Robin Hughes and his experimental team and Allan Runstedtler at Natural Resources Canada/CanmetENERGY for their support of this collaboration, for sharing valuable data from their 50kWth test facility, and for their extensive consultation on problem set up and data interpretation.

- This work was performed in support of the U.S. Department of Energy's Fossil Energy Crosscutting Technology Research Program. The Research was executed through the NETL Research and Innovation Center's Advanced Reaction Systems Field Work Proposal. The Research was supported in part by an appointment to the U.S. Department of Energy Postgraduate Research Program at the National Energy Technology Laboratory administered by the Oak Ridge Institute for Science and Education. Research performed by Leidos Research Support Team staff was conducted under the RSS contract 89243318CFE000003.

Disclaimer

• This work was funded by the Department of Energy, National Energy Technology Laboratory, an agency of the United States Government, through a support contract with Leidos Research Support Team (LRST). Neither the United States Government nor any agency thereof, nor any of their employees, nor LRST, nor any of their employees, makes any warranty, expressed or implied, or assumes any legal liability or responsibility for the accuracy, completeness, or usefulness of any information, apparatus, product, or process disclosed, or represents that its use would not infringe privately owned rights. Reference herein to any specific commercial product, process, or service by trade name, trademark, manufacturer, or otherwise, does not necessarily constitute or imply its endorsement, recommendation, or favoring by the United States Government or any agency thereof. The views and opinions of authors expressed herein do not necessarily state or reflect those of the United States Government or any agency thereof.